Deliverable 2.2 – Work Package 2:
Algorithms on characterising analytically resonance frequencies & power management.

WP2 leader	DTU
Authors	Luis Orellana
Dissemination level	Public
Website	http://innodc.org/
Grant Agreement number	765585
Due delivery	Month 18: 28 February 2019
Project dates	01/09/2017 – 31/08/2021

Deliverable description

The main objective of this deliverable is to develop algorithms and methods for characterising the resonances in grid connected VSC systems.

The interaction between the controller of power converters and poorly damped AC networks are identified causes of resonance oscillatory stability phenomena. Two methods to model grid-connected VSC systems to study stability are investigated: the state-space and the impedance based model. Validation has been carried out between the two methodologies by analyzing eigenvalues and singular values of the system. Furthermore, a time-domain simulation has been done to validate the state-space model with a non-linear MATLAB/Simulink model.

The details of the performed work are given in the attached paper submitted for publication, while the models are at UPC and available to the consortium members upon request.

Symposium Aalborg, Denmark
4th-7th June 2019

87

On resonance instabilities in VSCs connected to weak grids

L, ORELLANA, E, PRIETO-ARAUJO, L, SAINZ, M, CHEAH-MANE,
O, GOMIS-BELLMUT
CITCEA - Universitat Politècnica de Catalunya
Spain

SUMMARY

This paper addresses the resonance oscillatory stability phenomena studied in the literature and reported by network operators in grid-connected VSC systems. Negative interactions have been observed at different frequencies in these systems, causing the tripping of power converters (e.g. wind turbines or HVDC applications). The interaction between the controller of power converters and poorly damped AC networks are identified causes of these events.
This paper analyses two methods to model grid-connected VSC systems applied in the literature to study stability: the state-space and the impedance based model. Validation has been carried out between the two methodologies by analyzing eigenvalues and singular values of the system. Furthermore, a time-domain simulation has been done to validate the state-space model with a non-linear MATLAB/Simulink model.
The stability is studied in a base case system with a grid-connected VSC to the main AC grid via an LC circuit. A sensibility analysis of the strength of the grid and an analysis of sub-synchronous and harmonic oscillatory resonances is carried out.

KEYWORDS

"VSC", **"STABILITY"**, **"STATE-SPACE"**, **"IMPEDANCE BASED"**.

luis.orellana@upc.edu

1 INTRODUCTION

Grid-connected voltage source converters (VSCs) have been used to connect renewable energy resources located in remote areas where the short-circuit ratio (SCR) is small (SCR below 4), defined as weak grids. The interaction of these passive components with active elements has been reported to create oscillatory instabilities [1], [2], [3]. According to the frequency range this phenomena happens, they can be categorized into two large groups: harmonic and near-synchronous oscillatory instabilities.

Near-synchronous instabilities occur when the electrical network exchanges energy with the mechanical system of generators at one or more frequencies close to the synchronous frequency. However, some instabilities do not involve a mechanical interaction of any kind such as SSCI (Subsynchronous Control Interactions), where the interaction is between the control of the converter and elements of the weak network [4], [5]. According to the range of frequency, near-synchronous instabilities can be further be categorized into super-synchronous and sub-synchronous. Super-synchronous oscillations range 55 to 100 Hz and sub-synchronous oscillations range 25 to 45 Hz [6]. These type of instabilities might cause shaft fatigues and tripping of generators [3], [7].

Harmonics instabilities are caused by unstable or marginally stable controllers. Instabilities happen when the VSC control interacts with poorly damped resonances. The range of these instabilities is 0.1 to 2 kHz, and they might damage or reduce the life expectancy of sensitive equipment [1] and [3]. Frequent tripping of turbines and converters have also been reported [8].

Methods to model grid-connected VSC systems in order to study the instability phenomena used in the literature are state-space and impedance based modelling. Impedance based modelling is based on the impedance characterization of the system which can be expressed as a transfer function in the s-domain [9], [10]. On the other hand, state-space modelling represents it as a system of linear equations in the time domain, resulting in a state transition matrix which relates the inputs and the outputs of the system.

Both methodologies and a complete non-linear simulation model for validation purposes have been developed in MATLAB/Simulink . Results in the time domain have been compared between the non-linear and the state-space model. In addition, by computing the eigenvalues and the singular values, both models, impedance and state-space, have been compared.

Finally, a stability study for sub-synchronous and harmonic oscillatory instabilities have been carried out with both models. The analysis of sub-synchronous and harmonic resonances by looking at the singular values and the effect of reducing the strength of the network (weak grid) over the stability of the system.

2 SYSTEM MODEL

The testing system is a VSC power inverter connected to the grid through a LC circuit. The model of the power converter is an averaged two level converter, which uses vector control strategy with a cascaded controller (outer and inner loop) to control active power and AC voltage as illustrated in Fig. 1.

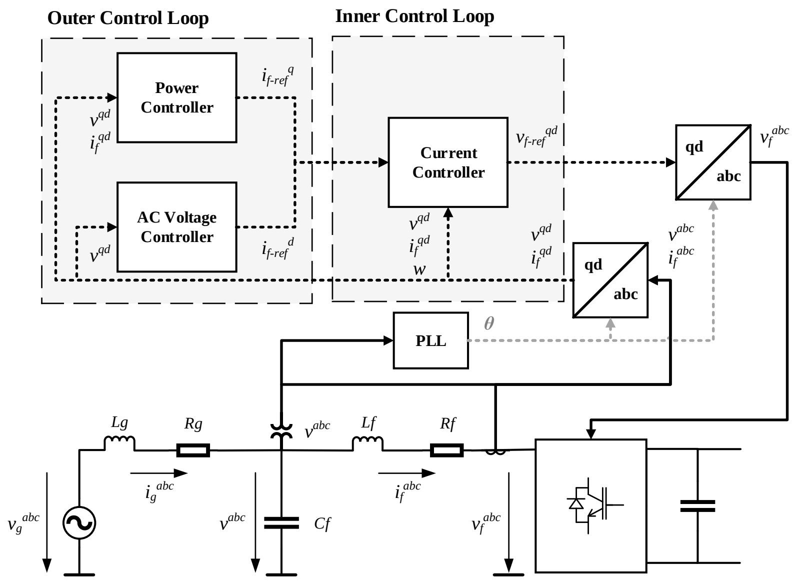

Figure 1: Grid-connected VSC system

2.1 Inner Loop Controller

The voltage at the converter terminals (ΔV_f) in the s-domain frame and the voltage reference output (V^c_{f-ref}) of the inner loop are:

$$\Delta V_f = \Delta V - (R_f + L_f s)\Delta I_f + j\omega L_f I_f \tag{1}$$

$$\Delta V^c_{f-ref} = \Delta V^c - F_{il}(I^c_{f-ref} - I^c_f) + j\omega L_f I^c_f \tag{2}$$

where $F_{il} = k_{p-il} + ki - il/s$ and the gains are $k_{p-il} = \dfrac{R_f}{\tau_{il}}$ and $k_{i-il} = \dfrac{L_f}{\tau_{il}}$ [11].

2.2 Outer loop controller

The outer loop controls active power with the q-component (i^c_{ref-q}) and AC voltage controller with the d-component (i^c_{ref-d}) as described in [12] for VSCs connected to weak grids. The outer loop control expressions are the following:

$$i^c_{ref-q} = F_{olp}(P_{ref} - P), \qquad P = \frac{3}{2}(v^c_q i^c_q + v^c_d i^c_d) \tag{3}$$

$$i^c_{ref-d} = F_{olv}(V_{ref} - V), \qquad V = \sqrt{(v^c_q)^2 + (v^c_d)^2} \tag{4}$$

where $F_{olp} = k_{p-olp} + k_{i-olp}/s$ and $F_{olv} = k_{p-olv} + k_{i-olv}/s$.

2.3 Phase-locked loop

The Phase-Locked Loop (PLL) provides the rotation angle of the three-phase voltage phase to relate the qd-component in the converter frame with the qd-components in the grid frame [13]. The angle can be obtained with the following expression.

$$\Delta\theta = -\frac{G_{pll}}{s + \Delta V_0 G_{pll}}\Delta V_d, G_{pll} = \frac{F_{pll}}{s + V_{0-q}F_{pll}} \tag{5}$$

where $F_{pll} = k_{p-pll} + k_{i-pll}/s$.

3 IMPEDANCE BASED MODEL

The impedance based model characterizes the elements of the system into impedances expressed as transfer functions in the s-domain. The system has been divided in three impedances: the convertes's impedance considering the control structure (Z_{vsc}); the shunt capacitance (Z_c); and the grid (Z_g) impedances as displayed in Fig. 2. The dynamic expressions in the three phase reference time-domain equations are expressed in the qd reference in the s-domain by applying the following transformation.

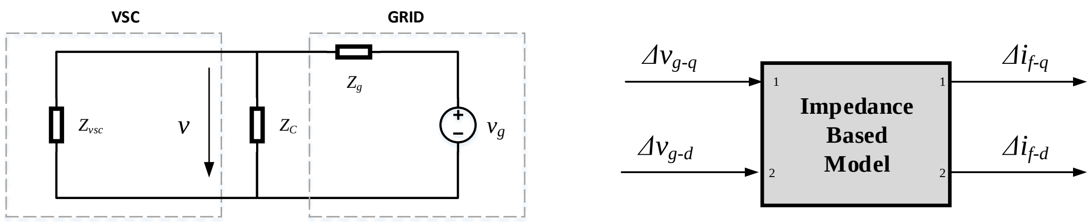

(a) (b)

Figure 2: VSC grid-connected impedance based model (a) equivalent diagram (b) transfer function

$$\begin{bmatrix} v_q & v_d \end{bmatrix}^T = \frac{2}{3} e^{j\omega t} \begin{bmatrix} 1 & e^{j4\pi/3} & e^{j2\pi/3} \end{bmatrix} \begin{bmatrix} v_a & v_b & v_c \end{bmatrix}^T \tag{6}$$

The transformation effect can be modelled as $e^{j\Delta\theta} \approx (1 + j\Delta\theta)$, where $\Delta\theta$ is the error angle between the angle of the system and the converter, where the steady state value of $\Delta\theta$ and v_{0-d} is expected to be 0. Therefore, the transformation and inverse transformation for voltage and current can be expressed as:

$$\begin{bmatrix} \Delta V_q^c \\ \Delta V_d^c \end{bmatrix} = \begin{bmatrix} 1 & 0 \\ 0 & 1 + G_{pll} V_{0-q} \end{bmatrix} \begin{bmatrix} \Delta V_q \\ \Delta V_d \end{bmatrix} \tag{7}$$

$$\begin{bmatrix} \Delta I_{f-q}^c \\ \Delta I_{f-d}^c \end{bmatrix} = \begin{bmatrix} \Delta V_{f-q} \\ \Delta I_{f-d} \end{bmatrix} + \begin{bmatrix} 0 & -G_{pll} V_{0-d} \\ 0 & G_{pll} V_{0-q} \end{bmatrix} \begin{bmatrix} \Delta V_q \\ \Delta V_d \end{bmatrix} \tag{8}$$

$$\begin{bmatrix} \Delta V_{f-q} \\ \Delta V_{f-d} \end{bmatrix} = \begin{bmatrix} \Delta V_{d-q}^c \\ \Delta V_{d-d}^c \end{bmatrix} + \begin{bmatrix} 0 & G_{pll} V_{0-d} \\ 0 & -G_{pll} V_{0-q} \end{bmatrix} \begin{bmatrix} \Delta V_q \\ \Delta V_d \end{bmatrix} \tag{9}$$

The current references can be defined as: $\Delta i_{ref-q}^c = -F_{olp} \Delta P$ and $\Delta i_{ref-d}^c = -F_{olv} \Delta V$, where the small signal power (ΔP) and ac voltage (ΔV) are the following:

$$\Delta P = \frac{3}{2} [(I_{f0-q}^c \Delta V_q^c + V_{0-q}^c \Delta I_{f-q}^c + I_{f0-d}^c \Delta V_d^c + V_{0-d}^c \Delta I_{f-d}^c)] \tag{10}$$

$$\Delta V = \frac{V_{0-q}^c \Delta V_q^c}{\sqrt{(V_{0-q}^c)^2 + (V_{0-d}^c)^2}} + \frac{V_{0-d}^c \Delta V_d^c}{\sqrt{(V_{0-q}^c)^2 + (V_{0-d}^c)^2}} \tag{11}$$

The output of the inner loop (voltage references) can be expressed as:

$$\begin{bmatrix} \Delta V_{ref-q}^c \\ \Delta V_{ref-d}^c \end{bmatrix} = \begin{bmatrix} \Delta V_{h-q}^c \\ \Delta V_{h-d}^c \end{bmatrix} - F_{il} \begin{bmatrix} \Delta I_{ref-q}^c \\ \Delta I_{ref-d}^c \end{bmatrix} + \begin{bmatrix} F_{il} & -\omega L_f \\ \omega L_f & F_{il} \end{bmatrix} \begin{bmatrix} \Delta I_{f-q}^c \\ \Delta I_{f-d}^c \end{bmatrix} \tag{12}$$

where $[\Delta V^c_{h-q}\ \ \Delta V^c_{h-d}]^T = H_v[\Delta V^c_q\ \ \Delta V^c_d]^T$ and $[\Delta V^c_{d-q}\ \ \Delta V^c_{d-d}]^T = F_D[\Delta V^c_{ref-q}\ \ \Delta V^c_{ref-d}]$. H_v and F_D are the delay and the feed-forward filter respectively. The converter and the grid AC side of the network be modelled as:

$$\begin{bmatrix}\Delta V_{f-q}\\ \Delta V_{f-d}\end{bmatrix} = \begin{bmatrix}\Delta V_{f-q}\\ \Delta V_{f-d}\end{bmatrix} + \begin{bmatrix}R_f+L_f s & \omega L_f\\ -\omega L_f & R_f+L_f s\end{bmatrix}\begin{bmatrix}\Delta I_{f-q}\\ \Delta I_{f-d}\end{bmatrix} \tag{13}$$

$$\Delta V = Z_{vsc}\Delta I_f \tag{14}$$

$$\Delta V = Z_c(\Delta I_g - \Delta I_f) \tag{15}$$

$$Z_c = \begin{bmatrix}C_f s & C_f\omega\\ -C_f\omega & C_f s\end{bmatrix} \tag{16}$$

$$\Delta V_g = \Delta V + Z_g\Delta I_g \tag{17}$$

$$Z_g = \begin{bmatrix}R_g+L_g s & \omega L_g\\ -\omega L_g & R_g+L_g s\end{bmatrix} \tag{18}$$

where $\Delta V = [\Delta V_q\ \ \Delta V_d]^T$, $\Delta I_f = [\Delta I_{f-q}\ \ \Delta I_{f-d}]^T$, $\Delta V_g = [V_{g-q}\ \ V_{g-d}]^T$, and $\Delta I_g = [\Delta I_{g-q}\ \ \Delta I_{g-d}]^T$.

4 STATE-SPACE MODEL

The state-space method represent the system in a set of linearized equations as in (20) and (21). Time-domain equations in the *abc* reference frame have been derived in the *qd* reference frame in the time domain by using (21).

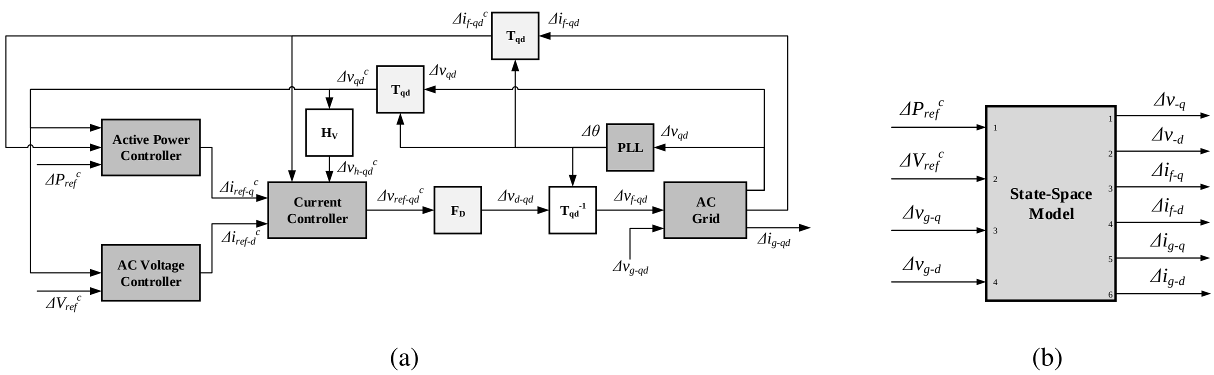

Figure 3: VSC grid-connected state-space model (a) equivalent diagram (b) state-space matrix

$$\Delta\dot{x} = \mathbf{A}\Delta x + \mathbf{B}\Delta u \tag{19}$$

$$\Delta y = \mathbf{C}\Delta x + \mathbf{D}\Delta u \tag{20}$$

$$\begin{bmatrix}v_q\\ v_d\end{bmatrix} = \frac{2}{3}\begin{bmatrix}\cos\theta & \cos(\theta-\frac{2\pi}{3}) & \cos(\theta+\frac{2\pi}{3})\\ \sin\theta & \sin(\theta-\frac{2\pi}{3}) & \sin(\theta+\frac{2\pi}{3})\end{bmatrix}\begin{bmatrix}v_a\\ v_b\\ v_c\end{bmatrix} \tag{21}$$

Where Δx are the state variables, Δy the output variables, and Δu the input variables. The transformation effect for Δv described in the impedance model can be derived in state-space as (22). Similar expression can be derived for Δi_f and Δv_f by changing the steady state values and applying the inverse of the matrix where applicable.

$$T_{qd} = \begin{bmatrix}\cos(\Delta\theta_0) & \sin(\Delta\theta_0) & -\sin(\Delta\theta_0)\Delta v_{0-q}+\cos(\Delta\theta_0)\Delta v_{0-d}\\ -\sin(\Delta\theta_0) & \cos(\Delta\theta_0) & -\cos(\Delta\theta_0)\Delta v_{0-d}+\sin(\Delta\theta_0)\Delta v_{0-d}\end{bmatrix} \tag{22}$$

The current references can be expressed in terms of a small signal variation in active power (ΔP_{ref}) and AC voltage (ΔV_{ref}) references, used for real-time simulations as it will be described in the results section.

$$\Delta i^{c}_{ref-q} = F_{olp}(\Delta P_{ref} - \Delta P) \tag{23}$$
$$\Delta i^{c}_{ref-d} = F_{olv}(\Delta V_{ref} - \Delta V) \tag{24}$$

Where ΔP and ΔV have been defined in (10) and (11). The inner loop's state-space matrices are in (25) and (26); and the AC side matrices are in (27) and (28).

$$\mathbf{A_{il}} = [\mathbf{0_{4x4}}] \qquad \mathbf{B_{il}} = [\mathbf{I_{4x4}}|\mathbf{0_{4x2}}] \tag{25}$$

$$\mathbf{C_{il}} = \begin{bmatrix} -k_{i-il} & 0 & k_{i-il} & 0 \\ 0 & -k_{i-il} & 0 & k_{i-il} \end{bmatrix} \quad \mathbf{D_{il}} = \begin{bmatrix} -k_{p-il} & 0 & k_{p-il} & -\omega L_f & 1 & 0 \\ 0 & -k_{p-il} & \omega L_f & k_{p-il} & 0 & 1 \\ \end{bmatrix} \tag{26}$$

$$\mathbf{A_{ac}} = \begin{bmatrix} -1/C_f & 0 & 0 & -\omega & 1/C_f & 0 \\ 0 & -1/C_f & \omega & 0 & 0 & 1/C_f \\ -R_f/L_f & -\omega & 1/L_f & 0 & 0 & 0 \\ \omega & -R_f/L_f & 0 & 1/L_f & 0 & 0 \\ 0 & 0 & -1/L_g & 0 & -Rg/L_g & -\omega \\ 0 & 0 & 0 & -1/L_g & \omega & -Rg/L_g \end{bmatrix} \tag{27}$$

$$\mathbf{B_{ac}} = \begin{bmatrix} 0 & 0 & 0 & 0 \\ 0 & 0 & 0 & 0 \\ -1/L_f & 0 & 0 & 0 \\ 0 & -1/L_f & 0 & 0 \\ 0 & 0 & 1/L_g & 0 \\ 0 & 0 & 0 & 1/L_g \end{bmatrix}, \mathbf{C_{ac}} = [\mathbf{I_{6x6}}], \mathbf{D_{ac}} = [\mathbf{0_{4x6}}] \tag{28}$$

5 STUDY CASE

The performance of the models is tested in this section. First, a comparison between the state-space and the non-linear model for a time simulation, and then a comparison of eigenvalues and singular values for impedance based and state-space. Finally, the study of harmonic and near-synchronous oscillatory resonances is studied for weak grids. The main parameters of the system are described in the following table.

Table 1: System parameters

Parameter	Symbol	Value	Units
Filter resistance	R$_f$	0.2372	Ω
Filter inductance	L$_f$	0.0750	H
Filter capacitance	C$_f$	10	μF
Feed-forward voltage filter	τ_{ffv}	1	ms
Delay	τ_d	100	μs

6 RESULTS AND DISCUSSION

A simulation in the time domain has been carried out of the non-linear and the linear state-space models for a SCR of the grid of 4. A step variation within the 15 percent in active power has been applied to both models as illustrated in Fig. 4.

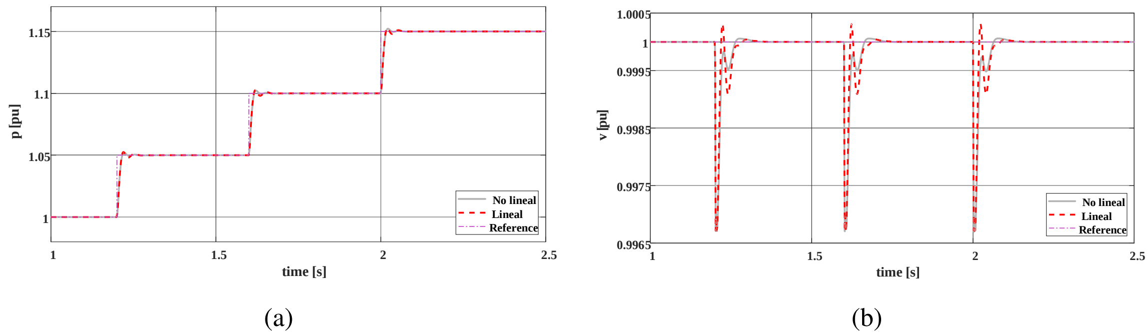

Figure 4: Non-linear and state-space models comparison (a) active power (b) AC voltage

The ratio of $\Delta v_g/\Delta i_f$ has been compared in eigenvalues and singular values between the state-space and impedance based model. The results are displayed in Fig. 5. It can be seen that both models have similar results.

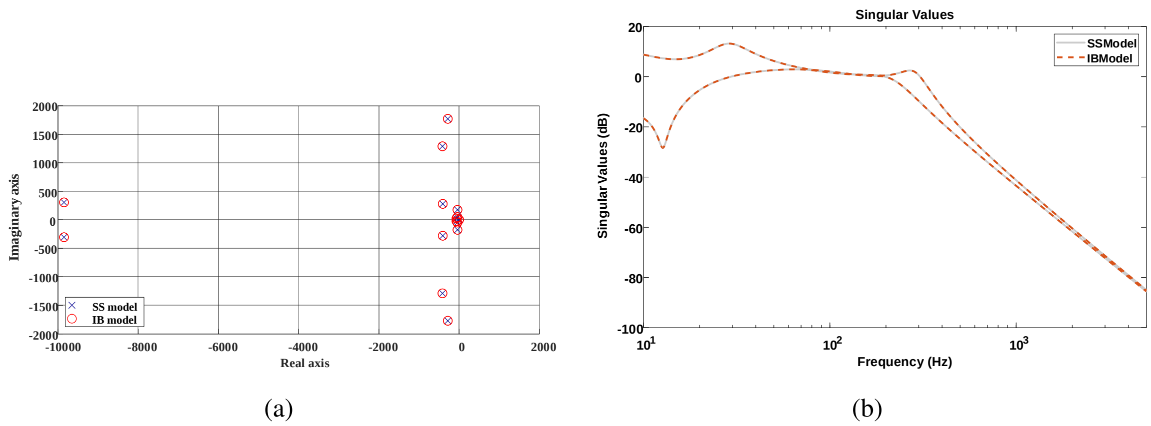

Figure 5: State-space and impedance based models comparison (a) eigenvalues (b) singular values

Oscillations have been observed in the AC voltage when the value of C_f is reduced from 10 to 1 μs . By looking at the singular values, it can be determined that the frequency of oscillation is approximately 26 Hz for sub-synchronous and around 755 Hz for harmonic oscillatory resonances (the complete state-space model has been used for this simulation, not the one reduced for the comparison part). The results by using singular values are shown in Fig. 6.
In addition, a sensibility analysis of the strength of the grid has been carried out. The SCR of the grid has been reduced from 5 to 1, and the system becomes unstable (poles with the real part above 0) from SCR below 3 as displayed in Fig. 7. Singular values indicate that sub-synchronous oscillatory resonances of a frequency around 25 Hz are the main cause of instability; furthermore, the linear model becomes unstable for 2.4 SCR which is higher than the non-linear model (2.2 SCR).

7 CONCLUSION

The results of comparing the state-space and impedance based modelling show that there is a good agreement between them. Further validation of the models has been achieved by comparing the state-space modelling with a non-linear simulink model. However, along the process some differences have been found. The most important ones are: the variation in active power

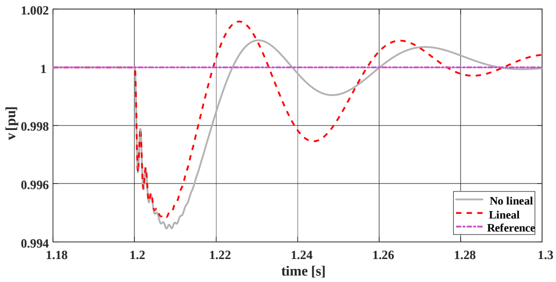

(a)

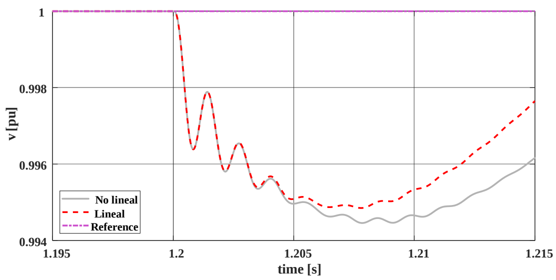

(b)

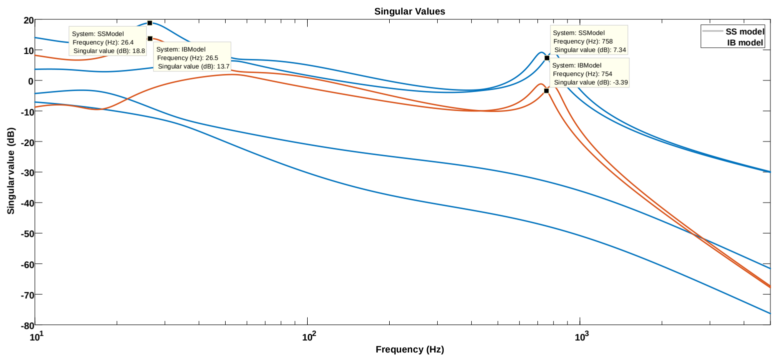

(c)

Figure 6: Oscillatory resonance instability (a) AC voltage harmonic and sub-synchronous oscillations (b) AC voltage harmonic oscillations (c) singular values

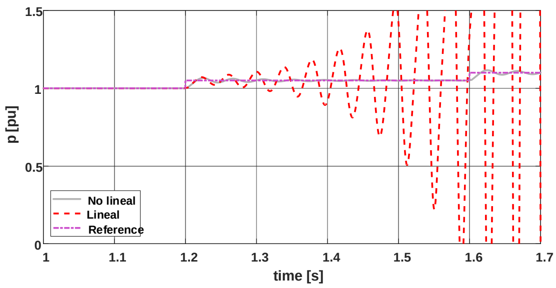

(a)

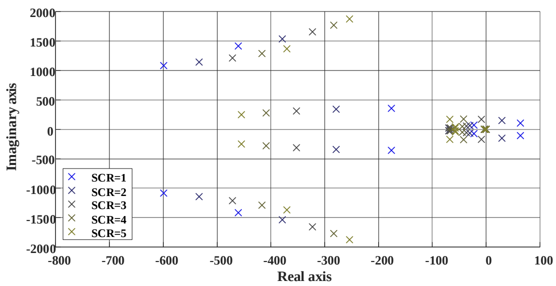

(b)

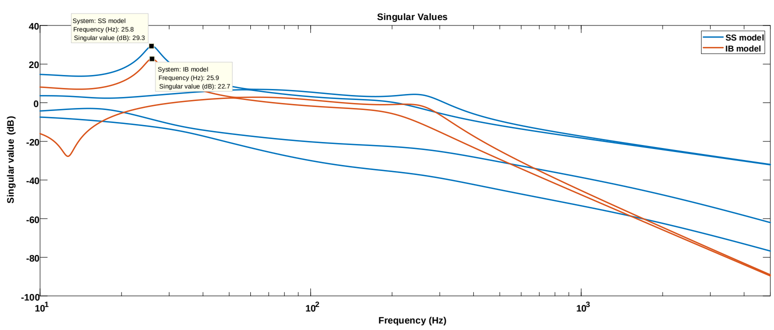

(c)

Figure 7: Sensibility analysis of the strength of the grid (a) time simulation (b) eigenvalues (c) singular values

and AC voltage references cannot be modelled in impedance based, and the controller characteristics of the impedance based are "hidden" inside the impedance of the converter (Z_{vsc}).
The stability assessment show that oscillatory resonances can be clearly identified with both models, similar results have been obtained for time domain simulation and by looking at the singular values for both models. By analyzing the eigenvalues, the instability of a system has been identified with both models, but for a low SCR the linearized model (impedance based and state-space) becomes unstable before the non-linear one.

BIBLIOGRAPHY

[1] F. D. Freijedo, S. K. Chaudhary, R. Teodorescu, J. M. Guerrero, C. L. Bak, L. H. Kocewiak, and C. F. Jensen, “Harmonic resonances in Wind Power Plants: Modeling, analysis and active mitigation methods,” in *2015 IEEE Eindhoven PowerTech*. IEEE, 6 2015, pp. 1–6.

[2] C. Buchhagen, C. Rauscher, A. Menze, and J. Jung, “BorWin1 - First Experiences with harmonic interactions in converter dominated grids,” *International ETG Congress 2015; Die Energiewende - Blueprints for the new energy age*, pp. 27–33, 2015.

[3] J. Sun, M. Li, Z. Zhang, T. Xu, J. He, H. Wang, and G. Li, “Renewable Energy Transmission by HVDC Across the Continent : System Challenges and Opportunities,” *Csee Journal of Power and Energy Systems*, vol. 3, no. 4, pp. 353–364, 2017.

[4] D. Van Hertem, O. Gomis-Bellmunt, and J. Liang, *HVDC Grids*, D. Van Hertem, O. Gomis-Bellmunt, and J. Liang, Eds. Hoboken, NJ, USA: John Wiley & Sons, Inc., 2 2016.

[5] G. D. Irwin, A. K. Jindal, and A. L. Isaacs, “Sub-synchronous control interactions between type 3 wind turbines and series compensated AC transmission systems,” in *2011 IEEE Power and Energy Society General Meeting*. IEEE, 7 2011, pp. 1–6.

[6] L. Sainz, M. Cheah-Mane, L. Monjo, J. Liang, and O. Gomis-Bellmunt, “Positive-Net-Damping Stability Criterion in Grid-Connected VSC Systems,” *IEEE Journal of Emerging and Selected Topics in Power Electronics*, vol. 5, no. 4, pp. 1499–1512, 2017.

[7] K. M. Alawasa, Y. A. R. I. Mohamed, and W. Xu, “Active mitigation of subsynchronous interactions between PWM voltage-source converters and power networks,” *IEEE Transactions on Power Electronics*, vol. 29, no. 1, pp. 121–134, 2014.

[8] C. Buchhagen, M. Greve, A. Menze, and J. Jung, “Harmonic Stability – Practical Experience of a TSO,” in *15th Wind Integration Workshop*, 2016.

[9] J. Sun, “Impedance-Based Stability Criterion for Grid-Connected Inverters,” *IEEE Transactions on Power Electronics*, vol. 26, no. 11, pp. 3075–3078, 11 2011.

[10] L. Harnefors, S. Member, M. Bongiorno, S. Member, and S. Lundberg, “Input-Admittance Calculation and Shaping for Controlled Voltage-Source Converters,” vol. 54, no. 6, pp. 3323–3334, 2007.

[11] L. Harnefors and H.-P. Nee, “Model-based current control of AC machines using the internal model\ncontrol method,” *IEEE Transactions on Industry Applications*, vol. 34, no. 1, pp. 133–141, 1998.

[12] A. Egea-Alvarez, S. Fekriasl, F. Hassan, and O. Gomis-Bellmunt, “Advanced Vector Control for Voltage Source Converters Connected to Weak Grids,” *IEEE Transactions on Power Systems*, vol. 30, no. 6, pp. 3072–3081, 11 2015.

[13] Se-Kyo Chung, “A phase tracking system for three phase utility interface inverters,” *IEEE Transactions on Power Electronics*, vol. 15, no. 3, pp. 431–438, 5 2000.